

HiSST: 4th International Conference on High-Speed Vehicle Science Technology 22 -26 September 2025, Tours, France



Transpiration Cooling with Porous Hastelloy X for Re-entry Space Vehicles

Jukyoung Shin*, Junhyeon Bae, Tae Young Kim Department of Mechanical and Automotive Engineering, Seoul National University of Science and Technology, 232 Gongneung-ro, Nowon-qu, Seoul 01811, Republic of Korea

Abstract

Vehicles undergoing atmospheric reentry and hypersonic flight are exposed to severe aerodynamic heating that exceeds the capabilities of conventional passive thermal protection systems. Transpiration cooling, which delivers coolant through a porous medium to absorb heat and establish a protective fluid barrier, offers high thermal efficiency relative to coolant mass and is therefore a promising solution for reusable aerospace vehicles. In this study, porous Hastelloy X specimens were fabricated by slurrybased compaction and sintering under applied pressures ranging from 0 to 81 MPa to examine how processing conditions affect pore structure and cooling performance under high-enthalpy heating. Porosity and permeability measurements showed that increasing compaction pressure reduced both total and open porosity, producing an overall ~60% decline in permeability due to diminished connectivity of flow pathways. Transpiration cooling experiments under a heat flux of ~1 MW/m² revealed that higher-pressure specimens maintained lower surface temperatures, demonstrating improved coolant utilization and enhanced thermal protection. These benefits, however, were offset by substantially greater hydraulic resistance, with the most compacted specimen exhibiting more than twice the pressure drop of the uncompressed sample. The results establish a fundamental trade-off: densification improves cooling uniformity and effectiveness but restricts fluid transport. This study provides quantitative design guidelines for optimizing porosity, permeability, and compaction pressure to balance thermal performance with hydraulic losses, supporting the development of next-generation transpiration cooling systems for hypersonic and reentry vehicles.

Keywords: transpiration cooling, re-entry space vehicle, phase change, porous media

1. Introduction

During atmospheric reentry and hypersonic flight, vehicles are exposed to extreme thermal environments caused by aerodynamic compression of the surrounding air and frictional heating at the surface. The resulting aerodynamic heating produces rapid temperature increases, particularly at leading edges and stagnation points, which pose critical challenges for the design of reliable thermal protection systems (TPS). Passive TPS, such as ablative coatings and ceramic composites, provide partial protection but cannot withstand the thermal loads of reentry for fully reusable spacecraft. Consequently, active cooling methods have been investigated as promising alternatives for achieving high durability and reusability in extreme environments [1].

Active cooling techniques explored for TPS include convective cooling, regenerative cooling, film cooling, and transpiration cooling. Convective cooling employs extended surface structures with flow-inducing devices to remove heat, and is widely used in applications such as electronics thermal management, combustion chambers, and power systems. Film cooling distributes a liquid layer over the heated surface, maintaining wall temperatures below the saturation temperature of the coolant. This approach has been implemented in gas turbines, rocket engines, nuclear reactors, and automotive systems, but requires complex fluid delivery mechanisms. Transpiration cooling, in contrast, introduces coolant through a porous wall exposed to the hot environment. As the coolant permeates the porous structure, it absorbs heat and exits uniformly across the surface, forming a fluid barrier that reduces convective and radiative heat transfer from the external high-enthalpy flow [2]. When a liquid coolant is used, vaporization provides additional heat absorption, resulting in a high effective heat transfer coefficient.

These combined effects enable transpiration cooling to achieve superior thermal protection efficiency per unit coolant mass compared to other methods, making it an attractive strategy for hypersonic vehicles, reusable spacecraft, rocket nozzles, and gas turbine blades [3].

Despite these advantages, significant challenges remain in fabricating porous structures that provide both effective cooling performance and sufficient thermomechanical strength under reentry conditions. Zhang et al. [4] demonstrated improved cooling performance using SiC ceramics with oriented microchannels fabricated through a template method, achieving high permeability and stable coolant delivery under heat fluxes up to 4 MW/m². However, long-term mechanical durability under thermal cycling was not addressed. Bellettre et al. [5] studied sintered stainless-steel plates cooled with liquid ethanol, showing that very low injection rates ($\sim 0.1\%$) provided over 95% cooling effectiveness, though precise characterization of evaporation and distribution remained challenging. Liu et al. [6] investigated stainless steel and bronze plates with different particle diameters in a heated wind tunnel, reporting higher cooling effectiveness for smaller pore sizes and more uniform temperature fields for bronze due to its higher thermal conductivity. These studies collectively highlight the influence of material selection, pore morphology, and coolant type on performance.

Another critical challenge is minimizing coolant consumption while suppressing flow instabilities. Luan et al. [7] showed that phase change in transpiration-cooled systems can induce thermal instabilities with large temperature and pressure fluctuations, preventing stable operation. Huang et al. [8] proposed combined transpiration and opposing jet cooling in porous stainless-steel struts, demonstrating enhanced leading-edge cooling but also identifying nonuniform coolant distribution as a limitation. Shin et al. [9] investigated Hastelloy X porous specimens under butane torch heating up to $220 \, \mathrm{kW/m^2}$, identifying four distinct flow regimes—liquid, partial phase-change, phase-change, and dry-out. They reported that the controlled phase-change regime provided the highest performance factor by balancing coolant efficiency and thermal protection, whereas partial phase-change conditions induced Ledinegg-type instabilities.

Although prior research has demonstrated the potential of transpiration cooling, important gaps remain. Fabrication techniques require optimization to ensure uniform pore distribution and mechanical robustness. In addition, systematic studies are needed to quantify operating conditions and to understand the influence of thermo-fluid instabilities on cooling performance. To address these issues, the present work investigates transpiration cooling using Hastelloy X porous specimens under simulated reentry conditions with a high-enthalpy heating device delivering $1.0 \, \text{MW/m}^2$. The study evaluates temperature distribution, vapor boundary layer development, pressure characteristics, and instability behavior across varying coolant injection rates. Furthermore, the durability of the porous medium is assessed through microstructural analysis following repeated thermal cycling tests, to establish design guidelines for reusable transpiration cooling systems.

2. Experiment

2.1. Porous specimens

Figure 1 illustrates the fabrication procedure for Hastelloy X specimens, a nickel-based alloy with hightemperature strength and oxidation resistance. The process consisted of four stages: mixing, compacting, debinding, and sintering. In the mixing stage, a binder solution was prepared by stirring polyvinyl alcohol (PVA) and deionized water at a weight ratio of 5:95 at 70°C for 10 min. PVA solution was then combined with Hastelloy X powder, composed of spherical particles with diameters of 50 -150 µm, at a weight ratio of 5:95 and mechanically mixed for 30 min to produce a slurry. For the compacting stage, a mold set consisting of an upper punch, lower punch, and cylindrical die was used. A mass of 14.7 g of slurry was introduced into a cavity made from a hardened steel die with an outer cylinder diameter of 15 mm and a lower punch. The slurry-filled mold was subjected to vibration tapping to enhance the packing efficiency of the powder-binder mixture. The applied vibration temporarily displaced the particles from their contact points, which reduced interparticle friction and enabled them to rearrange into more compact configurations. Simultaneously, the oscillatory motion facilitated the release of entrapped air bubbles located at the interfaces between powder particles and the binder solution. These bubbles were expelled through the narrow clearance between the mold wall and the punch. As a result, the process improved the uniformity of particle distribution and increased the densification of the green body, thereby ensuring the structural integrity necessary for subsequent

processing stages. After tapping, a uniaxial pressing machine applied pressures of 0, 25, 53, and 81 MPa for 1 min, producing cylindrical green bodies. The sintering curve for the preparation of the porous structure is shown in Figure 2. The green body is processed in a furnace where the temperature rises from room temperature to 600°C for 5 hr while supplied with Nitrogen gas at a flow rate of 3 LPM. During this process, known as the debinding process, the PVA is evaporated from the green body. With the green body inside, the temperature of the furnace rises to 1100°C for 5 hr and is maintained for 2 hr for sintering of the green body. During the sintering process, Nitrogen gas was supplied to the furnace at a flow rate of 5 LPM to protect the specimen from oxidation.

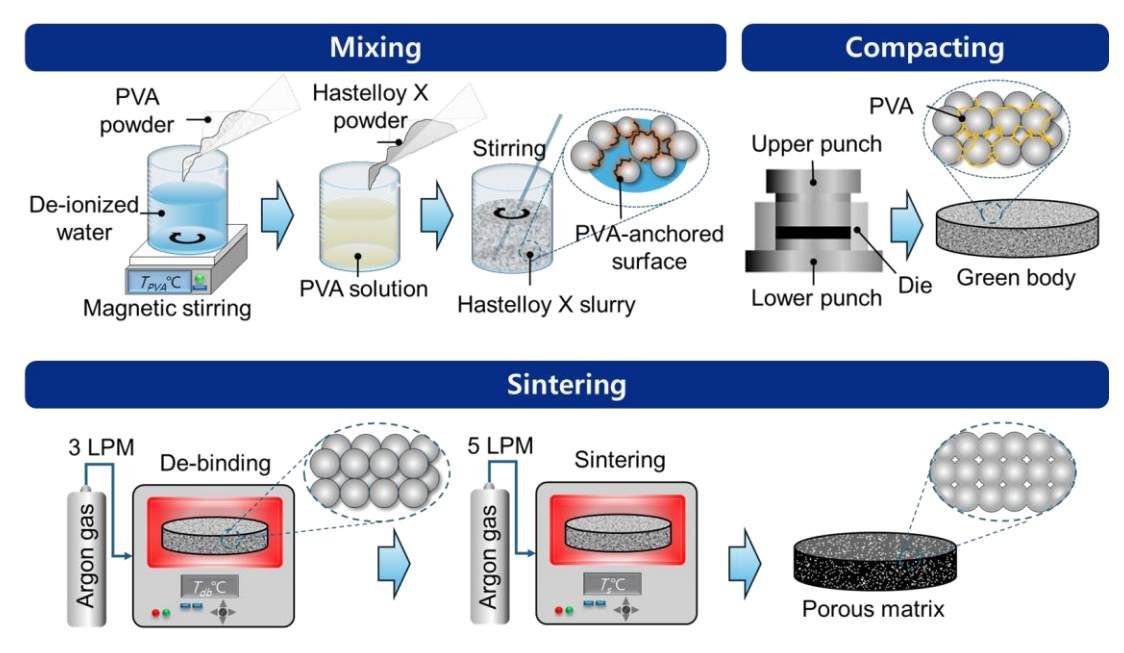


Fig 1. Specimen fabrication process

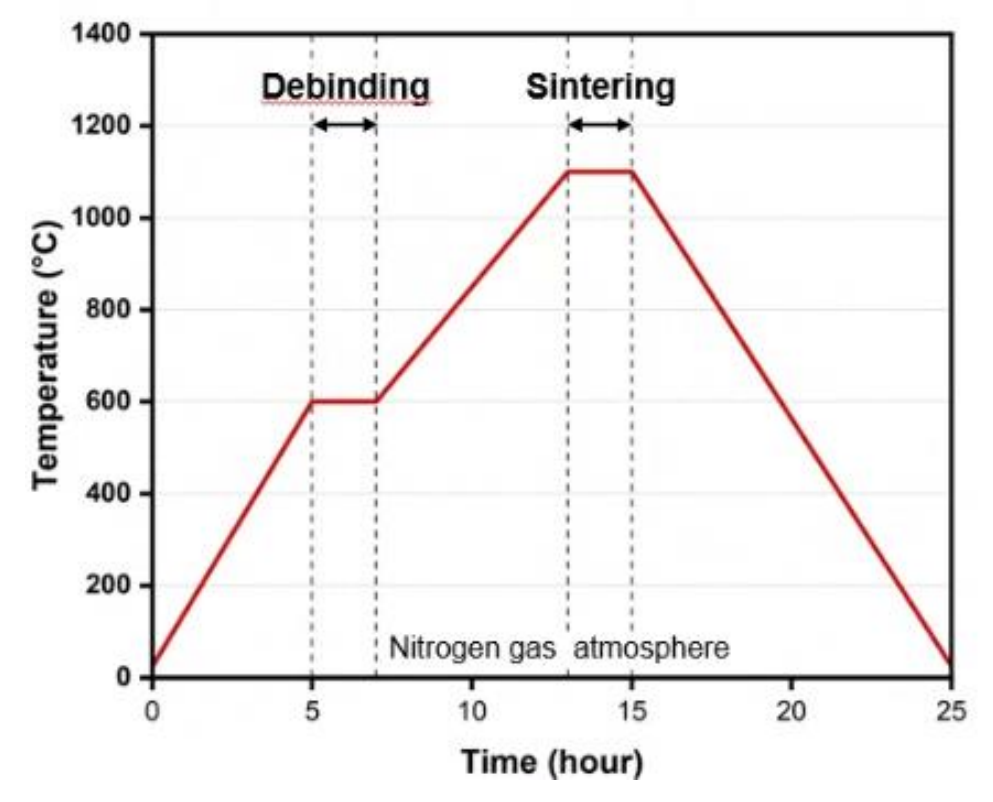


Fig 2. Sintering curve of the specimen

2.2. Characterize method of specimen

Figure 3 presents Hastelloy X specimens fabricated under four distinct compaction pressures, each initially formed as a cylinder with a diameter of 15 mm. Following sintering, the specimen height decreased with increasing compaction pressure, reflecting the higher green density achieved during pressing. To eliminate dimensional variation and ensure consistency in subsequent property and cooling performance evaluations, all specimens were precision-machined to a uniform height of 10 mm using a diamond cutter. The microstructure observed in the scanning electron microscope (SEM) image in Figure 2(b) shows that the spherical Hastelloy X particles are densely packed and metallurgically bonded, forming interparticle necks approximately 50 µm in width.

The porosity of the specimens was characterized in terms of both total and open porosity. Total porosity was determined using the gravimetric method, which relates the apparent density of the compact to the theoretical density of Hastelloy X, as expressed in Equation (1):

$$\varepsilon_{\text{total}} = 1 - \frac{m_{\text{s}}/V_{app}}{\rho_{\text{HX}}}$$
(1)

Where $\varepsilon_{\rm total}$ is the total porosity, $m_{\rm s}$ is the mass of the specimen, V_{app} is the apparent volume of the specimen, and $\rho_{\rm HX}$ is the theoretical density of Hastelloy. The open porosity was measured using the Archimedes method, which quantifies only the pore volume accessible to fluid infiltration, as expressed in Equation (2):

$$\varepsilon_{\text{open}} = \frac{(m_{\text{sat}} - m_{\text{dry,s}})/\rho_{\text{w}}}{V_{app}} \tag{2}$$

Where $\varepsilon_{\rm open}$ is the total porosity, $m_{\rm sat}$ is the saturated mass of the specimen after water immersion, $m_{\rm dry}$ is the dry mass of the specimen, ρ_w is the density of water under ambient conditions, and V_{app} is the apparent volume of the specimen. Comparing the total and open porosities provided an estimate of connectivity, which indicates the fraction of pores that form continuous fluid pathways and thus directly affect transpiration cooling performance.

The permeability of the specimens was quantified through water intrusion tests. The water permeability coefficient was calculated using Darcy's law, as expressed in Equation (3):

$$Q = \frac{\kappa A}{\mu} \frac{\Delta P}{L} \tag{3}$$

where Q represents the flow rate of deionized water flowing through the test sample (m^3/s), k is the permeability coefficient (m^2), μ denotes the viscosity of deionized water at room temperature ($N \cdot s/m^2$), L is the thickness of the sample (m), and ΔP is the pressure difference between the inside and outside of the sample (Pa).

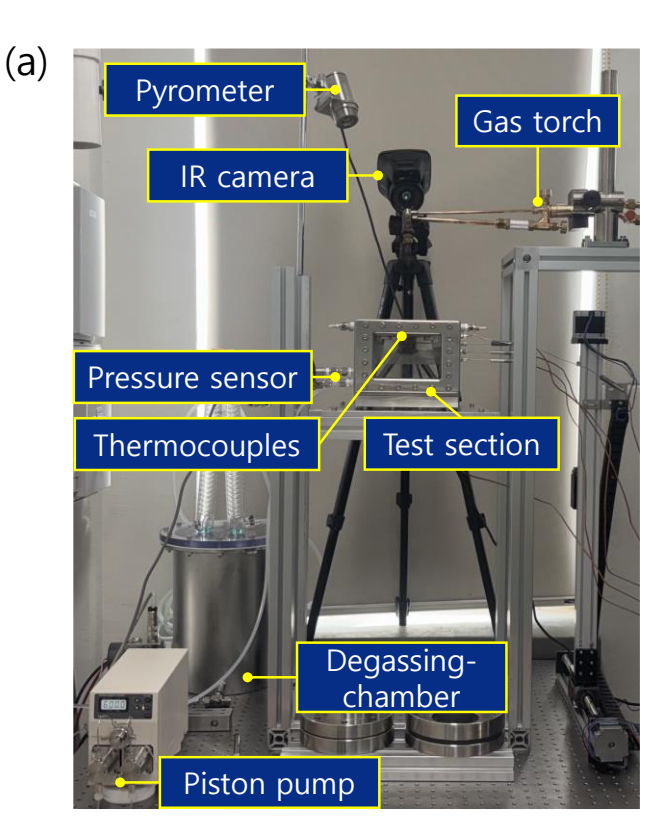


Fig 3. Image of the fabricated Hastelloy X specimens. (a) The macroscale view of the specimens, (b) an SEM image of the sintered particles

2.3. Experimental setup

The experimental setup and test section for evaluating the transpiration cooling performance of the porous specimen is shown in Figure 3. The heating system consisted of a gas torch fueled by oxygen and acetylene, designed to simulate the high heat flux encountered at the nose cone of a reentry vehicle. The applied heat flux was controlled by regulating the oxygen and acetylene flow rates through calibrated flow meters and by adjusting the distance between the flame and the specimen surface. Prior to testing, a heat flux measurement device was developed and experimentally validated to quantify the applied heat flux under these variables. Based on calibration results, a uniform heat flux of approximately 1 MW/m² was imposed on a 15 mm diameter heating surface when the torch-to-surface distance was set to 50 mm and the gas flow rates of oxygen and acetylene were maintained at 180 LPH.

The coolant supply system employed deionized water at room temperature, delivered to the porous specimen at constant flow rates using a piston pump (Intelligent SS, FLOM). To monitor the thermal and hydraulic responses of the specimen, multiple measurement devices were integrated into the test section. K-type thermocouples (KMQSS-125G-6, OMEGA) were inserted into the housing from the bottom and sides such that the sensor beads directly contacted the specimen surface, enabling accurate measurement of the solid temperature distribution. The top surface temperature of the specimen was measured using an infrared camera (Ti480 Pro, FLUKE), which provided non-intrusive measurements unaffected by the combustion flame. A differential pressure sensor (PSHE0100RCPG-NM, SENSYS) was used to record the system pressure drop during operation. Prior to exposure to the flame, each specimen underwent a pre-wetting step to ensure full saturation with coolant and to prevent structural damage under direct heating. Once heating commenced, the solid temperature exhibited a rapid rise due to the high thermal conductivity of the Hastelloy X matrix, while the coolant temperature increased more gradually because of its higher thermal resistance and heat capacity. The continuous inflow of coolant during this initial phase formed a liquid film at the surface, which was gradually displaced outward by the high-pressure flame. As heating progressed, the solid and fluid temperatures inside the specimen converged, and the liquid film stabilized at a thickness governed by the coolant flow rate. Steady-state conditions were defined when temperature fluctuations at the specimen bottom remained within ±0.3 °C for at least one minute. At this point, temperature and pressure data, along with infrared images, were collected over a five-minute period, and the time-averaged values were reported as the final results



Page | 5

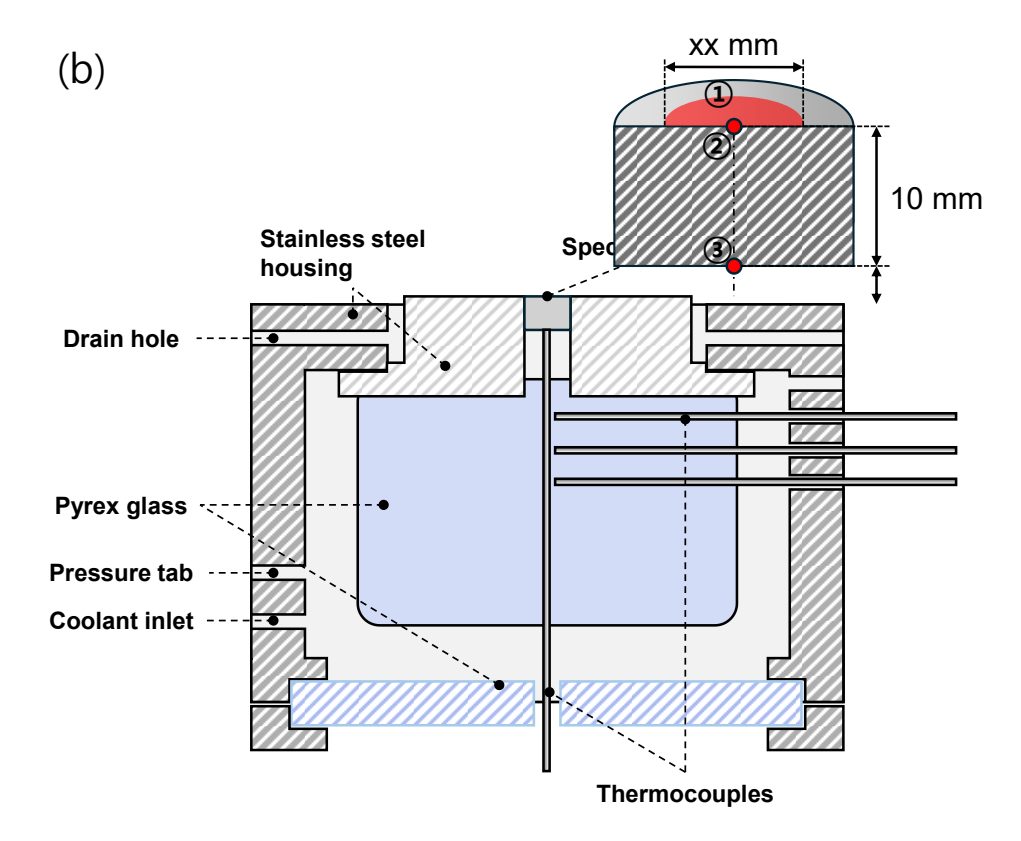


Fig 4. Schematics of (a) the experimental setup and (b) test section

3. Results

3.1. Properties of specimens

Figure 4 presents the measured porosity and permeability of the specimens as a function of compaction pressure. Both total porosity and open porosity decreased as the pressure increased. At 0 MPa, the total and open porosities were 39.2% and 33.4%, respectively, whereas at 85 MPa they declined to 35.1% and 28.1%. The difference between the two values widened with pressure, indicating a progressive reduction in pore connectivity caused by the formation of closed pores. This reduction can be attributed to the enlargement of particle contact areas and localized plastic deformation during compaction, which obstruct portions of the pore network. In addition, higher compaction pressures promote neck growth between particles, and subsequent sintering enhances diffusion at these contacts, further closing pores and amplifying the discrepancy between total and open porosity.

The permeability results also showed a consistent decline with compaction pressure, decreasing from $6.08 \times 10^{-12} \, \mathrm{m^2}$ at $0 \, \mathrm{MPa}$ to $2.51 \times 10^{-12} \, \mathrm{m^2}$ at $85 \, \mathrm{MPa}$, corresponding to nearly a 60% reduction in fluid transport capability. The strong correlation between the decrease in open porosity and the decline in permeability confirms that connectivity governs flow through the porous structure. As compaction densifies the specimen, the continuity of open channels is reduced, restricting fluid pathways. These results demonstrate that increasing compaction pressure improves structural densification but simultaneously diminishes permeability, highlighting a key trade-off in designing porous materials for transpiration cooling applications.

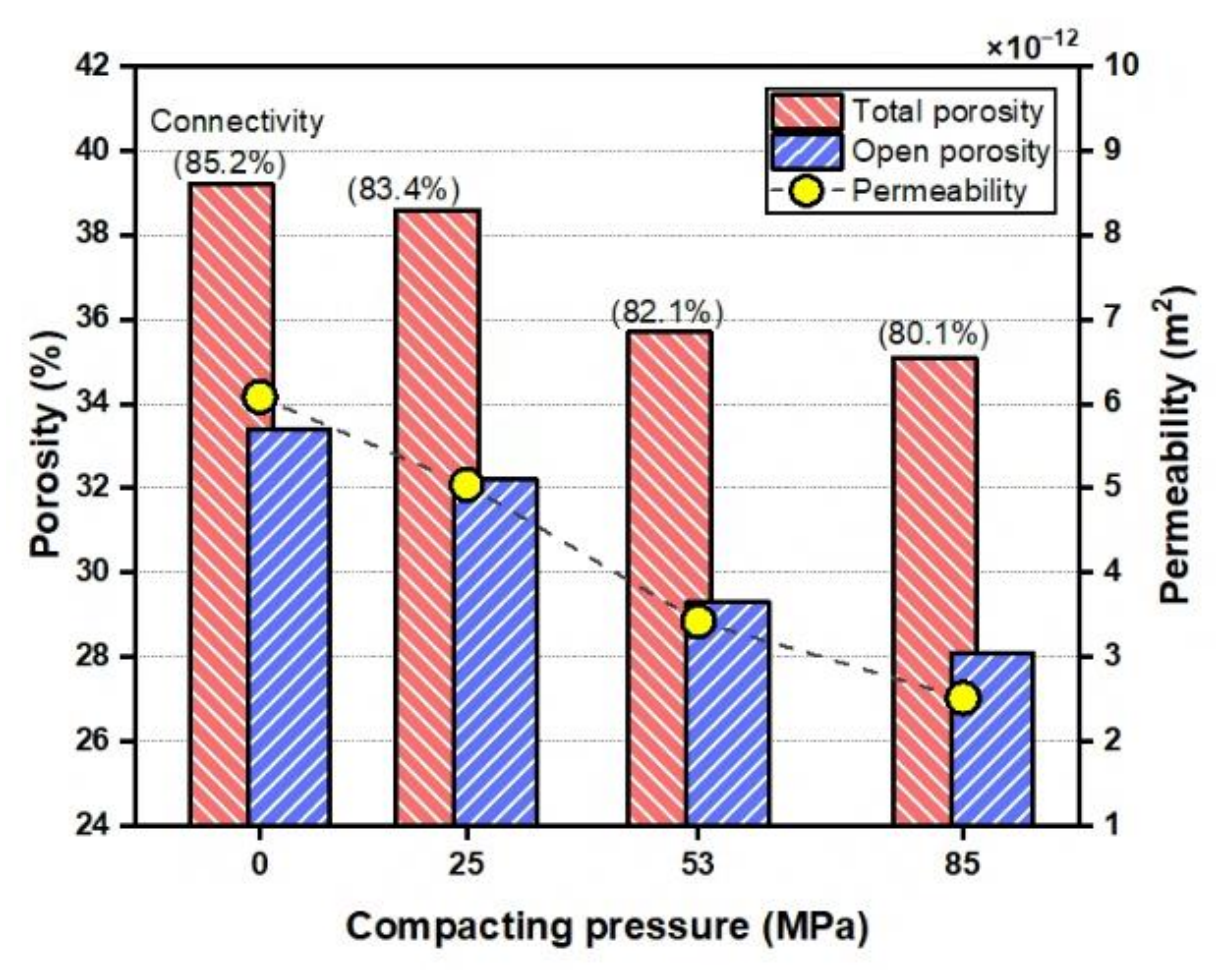


Fig 4. Properties of the fabricated Hastelloy X specimens

3.2. Transpiration cooling test

Figures 5 and 6 present the transpiration cooling performance and corresponding pressure drop of the specimens compacted under different pressures. As the coolant mass flux increased, the surface temperature of all specimens decreased sharply at low flow rates and then gradually stabilized before undergoing a second marked reduction near 0.65 kg/m²s. Specimens compacted at higher pressures (53 and 81 MPa) consistently exhibited lower surface temperatures than those compacted at lower pressures, indicating that densification during compaction improved the effectiveness of coolant utilization by promoting more uniform flow and enhanced heat absorption within the porous structure.

At the same time, the pressure drop results reveal the hydraulic penalty associated with densification. At low mass flux, specimens compacted at 81 MPa exhibited a pressure drop of approximately 75 kPa, more than double that of the uncompressed specimen (35 kPa), due to the reduced permeability and constricted flow pathways. With increasing mass flux, the pressure drop decreased sharply and then stabilized, although specimens with higher compaction pressure continued to show consistently greater resistance to flow. These results highlight a fundamental trade-off: higher compaction pressures enhance thermal performance by improving cooling uniformity but simultaneously increase hydraulic resistance, thereby limiting the ease of fluid transport. This interdependence between cooling efficiency and pressure loss must be carefully balanced in the design of porous media for transpiration cooling applications.

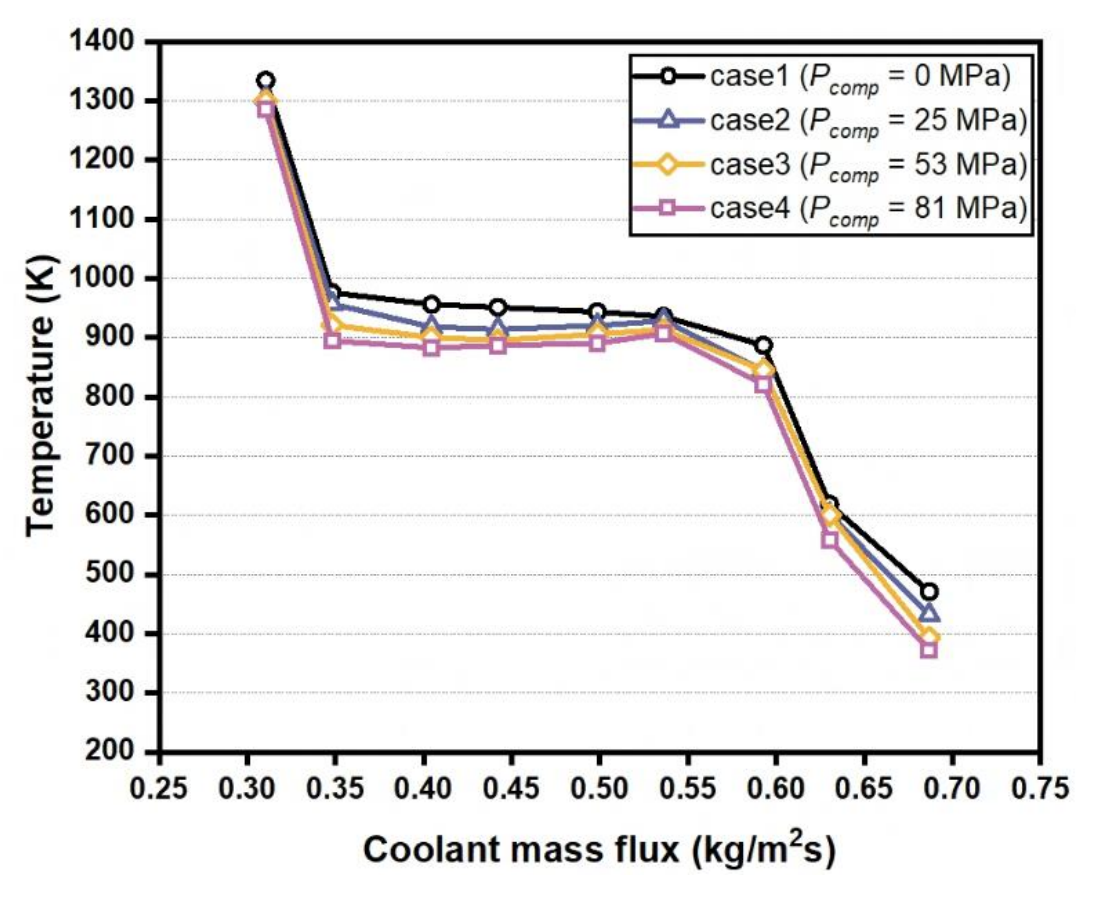


Fig 5. Temperature measured at the top surfaces of the specimens

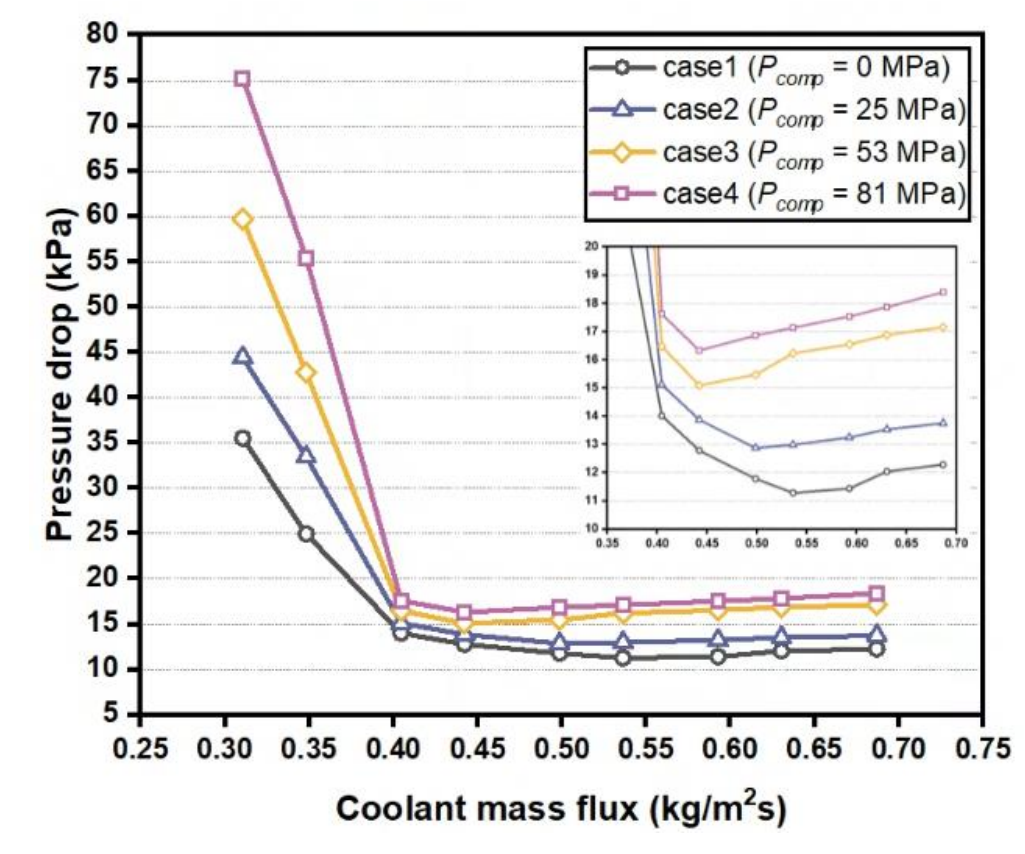


Fig. 6 The relationship between the pressure drop and mass flow rate of water coolant

4. Conclusions

This study provides a comprehensive framework for designing and evaluating transpiration cooling systems for aerospace applications. By developing a systematic fabrication approach for porous media, we established a reliable method to predict the effects of processing parameters on thermophysical properties. The experimental findings demonstrated that phase-change transpiration cooling effectively balances thermal protection and coolant consumption. Additionally, identifying four distinct cooling regimes and their associated flow instabilities offers critical insights into optimizing transpiration cooling performance. These results contribute to the advancement of high-efficiency thermal protection strategies for reusable space vehicles.

Acknowledgments

This work was supported by the "A nature-inspired high-efficiency solar energy collector mimicking energy metabolic mechanism of plants" funded by the National Research Foundation (NRF, 2022R1C1C1005922), Republic of Korea, and this work was also supported by Korea Research Institute for defense Technology planning and advancement(KRIT) grant funded by the Korea government (DAPA(Defense Acquisition Program Administration)) (No.KRIT-CT-22-030, Reusable Unmanned Space Vehicle Research Center, 2025).

References

- 1. Zhang, Li, Zuo, Oin, Cheng, Feng, Bao.: Research progress on active thermal protection for hypersonic vehicles. Ann. Mat. Pura Appl. 169, 321-354 (1995). Progress in Aerospace Sciences (2020). https://doi.org/10.1016/j.paerosci.2020.100646
- 2. Mi, Q., Yi, S. H., Gang, D. D., Lu, X. G., & Liu, X. L.: Research progress of transpiration cooling for aircraft thermal protection (2024). Applied Thermal Engineering. https://doi.org/10.1016/j.applthermaleng.2023.121360
- 3. Wang, Y., Wang, L., Zhou, Y., Luo, Z., Xie, W., Liu, Q., ... & Du, M.: Research progress on transpiration cooling technology in force-thermal concentrated environments (2025). International Journal of Heat and Mass Transfer. https://doi.org/10.1016/j.ijheatmasstransfer.2024.126262
- 4. Zhang, B., Li, Y., Lin, A., Gao, Y., Liu, B., & Fan, X.: Experimental investigation on transpiration cooling performance of porous ceramic with oriented channels (2025). Acta Astronautica. https://doi.org/10.1016/j.actaastro.2025.07.020
- 5. Bellettre, J., Bataille, F., Lallemand, A., & Andoh, H. Y. Studies of the transpiration cooling through a sintered stainless steel plate (2005). Experimental heat transfer. https://doi.org/10.1080/08916150590884835
- 6. Liu, Y. Q., Jiang, P. X., Xiong, Y. B., & Wang, Y. P. Experimental and numerical investigation of transpiration cooling for sintered porous flat plates (2013). Applied Thermal Engineering. https://doi.org/10.1016/j.applthermaleng.2012.08.028
- 7. Luan, Y., He, F., Wang, J., Wu, Y., & Zhu, G. An experimental investigation on instability of transpiration cooling with phase change (2020). International Journal of Thermal Sciences. https://doi.org/10.1016/j.ijthermalsci.2020.106498
- 8. Huang, G., Zhu, Y., Liao, Z., Lu, T., Jiang, P. X., & Huang, Z. Experimental study on combined cooling method for porous struts in supersonic flow (2018). Journal of Heat Transfer. https://doi.org/10.1115/1.4037499
- 9. Shin, J., Bae, J., Kim, S. J., & Kim, T. Y. Flow regimes and flow instability of transpiration cooling (2025).International Journal of Heat and Mass Transfer. https://doi.org/10.1016/j.ijheatmasstransfer.2025.127457